# Test of a Multiple Time Scale Formalism Applied to the Nonlinear Evolution of Negative-energy Modes

D. Pfirsch and F. Pohl

IPP 6/312 March 1993


MAX-PLANCK-INSTITUT FÜR PLASMAPHYSIK

8046 GARCHING BEI MÜNCHEN

MAX-PLANCK-INSTITUT FÜR PLASMAPHYSIK

GARCHING BEI MÜNCHEN

# Test of a Multiple Time Scale Formalism Applied to the Nonlinear Evolution of Negative-energy Modes

D. PFIRSCH AND F. POHL

IPP 6/312 March 1993

*Die nachstehende Arbeit wurde im Rahmen des Vertrages zwischen dem Max-Planck-Institut für Plasmaphysik und der Europäischen Atomgemeinschaft über die Zusammenarbeit auf dem Gebiete der Plasmaphysik durchgeführt.*

# Test of a Multiple Time Scale Formalism Applied to the Nonlinear Evolution of Negative-energy Modes

D. Pfirsch and F. Pohl
Max-Planck-Institut für Plasmaphysik
EURATOM Association
D-8046 Garching, F. R. Germany

**Abstract**

A multiple time scale formalism in three-wave interaction with negative-energy modes is applied to the structurally similar problem of a charged particle on an axially symmetric parabolic hill ($V = -(x^2 + y^2)/2$) with a small potential perturbation $\delta V = -4\epsilon x^3/3$ , $\epsilon << 1$ , and a sufficiently strong magnetic field in the $z$-direction. The multiple time scale solutions of first-order in $\epsilon$ are compared with the linearized solutions as well as the numerical solutions. In the light of the multiple time scale formalism the usual linearized theory should be valid only up to times of order 1, whereas the multiple time scale solutions of first-order in $\epsilon$ can be expected to be valid up to times of order $1/\epsilon$ . The linearized theory of the particle-on-a-hill problem predicts stability and allows positive and negative energy modes. For a resonance situation given essentially by the gyrofrequency being twice the drift frequency, a multiple time scale formalism applied to the nonlinear theory predicts explosive instability, except for some special cases. Explosive instability is also found numerically for certain initial conditions with dominant nonlinear force. However, for initial values with $x^2 + y^2$ and $\dot{x}^2 + \dot{y}^2$ of order 1 the nonlinear force is initially not dominant. In this case the multiple time scale solutions and the numerical solutions agree fairly well for the initial phase, lasting for a time interval of order $1/\epsilon$; then the multiple time scale solutions explode and the numerical solutions run away exponentially.

# 1 Introduction

In 1925 Cherry [1] discussed two one-dimensional oscillators of positive and negative energy that are nonlinearly coupled in a special way. He obtained for the case of third-order resonance a class of exact solutions of the nonlinear equations showing explosive instability independent of the strength of the nonlinearity and the initial amplitudes. One of the present authors reformulated and generalized Cherry's model [2] to three oscillators with a Hamiltonian essentially given by

$$H = \sum_{k=1}^{3} \omega_k \xi_k^* \xi_k + \alpha\, \xi_1 \xi_2 \xi_3 + \alpha^*\, \xi_1^* \xi_2^* \xi_3^* , \tag{1}$$

where

$$\xi_k = \frac{1}{\sqrt{2}} (p_k + i\, q_k) ; \tag{2}$$

$k$ is the oscillator number. $i\, \xi_k^*$ is the momentum canonically conjugate to $\xi_k$ . In quantum mechanical language one can call $\xi_k^*$ a creation operator for quanta possessing the energy $\omega_k$ and $\xi_k$ the corresponding annihilation operator. If there is resonance corresponding to the *conservation law*

$$\omega_1 + \omega_2 + \omega_3 = 0 , \tag{3}$$

then a three-parameter set of solutions to the equations of motion corresponding to the Hamiltonian (1) is

$$\xi_k = \left(\frac{i\alpha^*}{|\alpha|}\right)^{1/3} \frac{1}{\beta - |\alpha|\, t}\, e^{i\omega_k t + i\varphi_k} , \qquad \sum_{k=1}^{3} \varphi_k = 0 . \tag{4}$$

$\beta$ and the $\varphi_k$'s are constants of integration.

A more general system would, in addition to the kind of nonlinear terms occurring in the Hamiltonian (1), contain other "three-wave interaction" terms which are not resonant for $\omega_i'$s satisfying eq. (3). They would vanish by averaging over time. One can therefore speculate that these terms are less important than the resonant ones and that the latter still lead to unstable behaviour.

A method which introduces a certain kind of time averaging is the multiple time scale formalism. In this paper a simple physical example is treated which implies linear positive- and negative-energy modes and resonant as well as non-resonant coupling terms. The example is a charged particle on a hill characterized by the potential

$$U(x,y) = -\frac{1}{2}(x^2 + y^2) - \frac{4\epsilon}{3}x^3 , \tag{5}$$

where $\epsilon$ will be used as a smallness parameter. A contour line plot of the potential $U(x,y)$ is shown in Fig. 1. Superimposed is a constant magnetic field $B$ in the $z$-direction. For $B > 2$ the linear problem ($\epsilon = 0$) has only oscillatory solutions, half of them possessing positive energy and half of them negative energy. The first ones represent essentially gyro motions and the second ones drift motions. Resonance means that the frequency of the positive-energy mode is twice the frequency of the negative-energy mode.

In Sec. 2 the problem is solved to first order in $\epsilon$ by applying a multiple time scale formalism. It can be expected that this order is valid for time intervals of order $1/\epsilon$ if the initial values for $x^2 + y^2$ and $\dot{x}^2 + \dot{y}^2$ are of order 1. Section 3 presents a comparison between the approximate solutions thus obtained and numerical solutions.

## 2 The particle on a hill solved by multiple time scale formalism

With

$$\zeta = x + i\,y \tag{6}$$

the motion of a charged particle in the potential (5) and a superimposed constant magnetic field in the $z$-direction obeys the differential equation

$$\ddot{\zeta} + i\,B\,\dot{\zeta} - \zeta = \epsilon\,(\zeta + \zeta^*)^2 . \tag{7}$$

Multiple time scale formalism means the following expansion:

$$\zeta = \sum_{\nu=0}^{\infty} \epsilon^\nu\, \zeta_\nu(\tau_0, \tau_1, \dots) \tag{8}$$

with

$$\tau_\lambda = \epsilon^\lambda t , \qquad \frac{d}{dt} = \sum_{\lambda=0}^{\infty} \epsilon^\lambda \frac{\partial}{\partial \tau_\lambda} .$$

In lowest order in $\epsilon$ we have

$$\frac{\partial^2 \zeta_0}{\partial \tau_0^2} + i B \frac{\partial \zeta_0}{\partial \tau_0} - \zeta_0 = 0 . \tag{9}$$

This equation has the general solution

$$\zeta_0 = a_+(\tau_1, ...) e^{-i\omega_+ \tau_0} + a_-(\tau_1, ...) e^{-i\omega_- \tau_0} \tag{10}$$

with

$$\omega_\pm = \frac{B}{2} \pm \sqrt{\frac{B^2}{4} - 1} . \tag{11}$$

For $B > 2$ both frequencies are real. For large $B$ the term with $\omega_+$ describes essentially a gyro motion, and the term with $\omega_-$ a drift motion. The Lorentz force is compensated in the case of gyro motion by the centrifugal force and in the case of drift motion by the "hill" force from the potential (5). The energies of the $\omega_+-$ and $\omega_-$ motions are

$$E_\pm = |a_\pm|^2 \sqrt{\frac{B^2}{4} - 1} \left( \sqrt{\frac{B^2}{4} - 1} \pm \frac{B}{2} \right) , \tag{12}$$

and thus we have

$$E_+ > 0 \quad , \quad E_- < 0 . \tag{13}$$

In the following we consider the third-order resonance case

$$\omega_+ = 2 \omega_- , \tag{14}$$

which requires

$$B = \frac{3}{\sqrt{2}} \tag{15}$$

and

$$\omega_+ = \sqrt{2} \quad , \quad \omega_- = \frac{1}{\sqrt{2}} . \tag{16}$$

The first-order equation resulting from eq. (7) is

$$\frac{\partial^2 \zeta_1}{\partial \tau_0^2} + 2 \frac{\partial^2 \zeta_0}{\partial \tau_0 \, \partial \tau_1} + i B \frac{\partial \zeta_1}{\partial \tau_0} + i B \frac{\partial \zeta_0}{\partial \tau_1} - \zeta_1 = (\zeta_0 + \zeta_0^*)^2 . \tag{17}$$

This equation can be solved by means of the Green's function

$$G(\tau_0 - \tau_0') \;=\; \frac{i}{\omega_+ - \omega_-}\left(e^{-i\omega_+(\tau_0-\tau_0')} \;-\; e^{-i\omega_-(\tau_0-\tau_0')}\right) for\ \tau > \tau_0' \,. \quad (18)$$

For $\zeta_1$ vanishing at $\tau_0 = 0$ we have

$$\zeta_1 \;=\; \int_0^{\tau_0} d\tau_0' \,\frac{i}{\omega_+ - \omega_-}\left(e^{-i\omega_+(\tau_0-\tau_0')} \;-\; e^{-i\omega_-(\tau_0-\tau_0')}\right) \times$$
$$\left\{(\zeta_0 + \zeta_0^*)^2 \;-\; 2\,\frac{\partial^2\zeta_0}{\partial\tau_0\,\partial\tau_1} \;-\; i\,B\,\frac{\partial\zeta_0}{\partial\tau_1}\right\}_{\tau_0=\tau_0'} . \quad (19)$$

If the resonance condition (14) holds, the integral leads to contributions to $\zeta_1$ which increase indefinitely with $\tau_0$. The $\tau_1$-dependence of $\zeta_0$ can, however, and must be chosen such that these secular terms vanish. This condition, with the $\omega'$s given by eqs. (16), leads to the following equation for the amplitudes $a_+$ and $a_-$ :

$$a_-^2 \;+\; \frac{i}{\sqrt{2}}\,\frac{\partial a_+}{\partial\tau_1} \;=\; 0 \quad , \quad 2a_+a_-^* \;-\; \frac{i}{\sqrt{2}}\,\frac{\partial a_-}{\partial\tau_1} \;=\; 0\,. \quad (20)$$

We first observe that there exists a Cherry-like two-parameter set of solutions to these equations (20), namely

$$a_- \;=\; \frac{1}{2}\,\frac{e^{i\varphi}}{\tau_1 - T} \quad , \quad a_+ \;=\; -\,\frac{i}{2\sqrt{2}}\,\frac{e^{2i\varphi}}{\tau_1 - T}\,, \quad (21)$$

where $\varphi$ and $T$ are constants of integration. The initial values for $x, y,\ \dot{x}, \dot{y}$ belonging to these solutions are to lowest order in $\epsilon$

$$x_0 \;=\; -\,\frac{cos\varphi}{2T} \;-\; \frac{sin2\varphi}{2\sqrt{2}\,T} \quad , \quad y_0 \;=\; -\,\frac{sin\varphi}{2T} \;+\; \frac{cos2\varphi}{2\sqrt{2}\,T} \quad (22)$$

$$\dot{x}_0 \;=\; -\,\frac{sin\varphi}{2\sqrt{2}\,T} \;+\; \frac{cos2\varphi}{2T} \quad , \quad \dot{y}_0 \;=\; \frac{cos\varphi}{2\sqrt{2}\,T} \;+\; \frac{sin2\varphi}{2T}\,.$$

## 2.1 General solution of eqs. (20)

One can also find the general solution of eqs. (20). Multiplication of the second equation by $a_-$ yields

$$\frac{\partial}{\partial\tau_1}\, a_-^2 \;=\; -\, i\, 4\sqrt{2}\; a_+\, |a_-|^2\;. \tag{23}$$

Taking the time derivative of the first equation (20), one obtains

$$\frac{\partial^2 a_+}{\partial\tau_1^2} \;=\; i\,\sqrt{2}\frac{\partial}{\partial\tau_1}\, a_-^2 \;=\; 8\; a_+\, |a_-|^2 \;=\; 4\,\sqrt{2}\; a_+\, |\frac{\partial a_+}{\partial\tau_1}|\;. \tag{24}$$

Let us write

$$a_+ \;=\; A\, e^{i\phi} \tag{25}$$

with $A$ and $\phi$ real. We further introduce the notation

$$\cdot \;=\; \frac{\partial}{\partial\tau_1}\;; \tag{26}$$

then we have

$$|\frac{\partial a_+}{\partial\tau_1}| \;=\; +\,\sqrt{\dot{A}^2 + \dot{\phi}^2 A^2} \tag{27}$$

with positive sign because the left-hand side is a modulus and therefore positive. Thus eq. (24) becomes

$$\ddot{A} \;+\; 2i\dot{\phi}\dot{A} \;-\; \dot{\phi}^2 A \;+\; i\,\ddot{\phi}A \;=\; 4\sqrt{2}\; A\,\sqrt{\dot{A}^2 + \dot{\phi}^2 A^2}\;. \tag{28}$$

The real part of this equation is

$$\ddot{A} \;-\; \dot{\phi}^2 A \;=\; 4\sqrt{2}\; A\,\sqrt{\dot{A}^2 + \dot{\phi}^2 A^2} \tag{29}$$

and the imaginary part

$$2\dot{\phi}\dot{A} \;+\; \ddot{\phi}A \;=\; 0\;. \tag{30}$$

The latter equation has a first integral

$$\dot{\phi} \;=\; \frac{\gamma}{A^2} \tag{31}$$

with constant $\gamma$. Inserting eq. (31) into eq. (29) yields an equation for $A$ alone:

$$\ddot{A} - \frac{\gamma^2}{A^3} = 4\sqrt{2}\, A \sqrt{\dot{A}^2 + \frac{\gamma^2}{A^2}}\,. \tag{32}$$

From this relation it is seen that

$$sign\ \ddot{A} = sign\ A\,, \tag{33}$$

which means that unstable solutions always exist, especially for initial conditions with $sign\ \dot{A} = sign\ A$ . Multiplying eq. (32) by $2\dot{A}$, one obtains

$$\frac{\partial}{\partial \tau_1}\left(\dot{A}^2 + \frac{\gamma^2}{A^2}\right) = 4\sqrt{2}\sqrt{\dot{A}^2 + \frac{\gamma^2}{A^2}}\,\frac{\partial A^2}{\partial \tau_1}\,. \tag{34}$$

Integration over $\tau_1$ yields

$$+\sqrt{\dot{A}^2 + \frac{\gamma^2}{A^2}} = 2\sqrt{2}\,(A^2 + C)\,. \tag{35}$$

The constant $C$ can be expressed by the initial values $A_0$ , $\dot{A}_0$ of $A$ and $\dot{A}$:

$$C = -A_0^2 + \frac{1}{2\sqrt{2}}\sqrt{\dot{A}_0^2 + \frac{\gamma^2}{A_0^2}}\,. \tag{36}$$

Equation (35) can also be written as

$$\frac{1}{2}\,\dot{A}^2 + \frac{\gamma^2}{2\,A^2} - 4\,(A^2 + C)^2 = 0\,. \tag{37}$$

Formally eq. (37) is the energy of a "particle" with the coordinate $A$ in the potential

$$V(A) = \frac{\gamma^2}{2\,A^2} - 4\,(A^2 + C)^2\,. \tag{38}$$

The Cherry-like solutions (21) are obtained with

$$\gamma = 0\,, \qquad \phi = 2\varphi - \frac{3}{2}\,\pi\,, \qquad A_0 = \frac{1}{\sqrt{8}\,T}\,, \qquad \dot{A}_0 = \frac{1}{\sqrt{8}\,T^2}\,, \tag{39}$$

which implies $C = 0$ from eq. (36).

## 2.2 The case $\gamma = 0$

This case is more general than the Cherry-like case of eq. (39) with $\gamma$ and $C$ equal to zero and can be solved exactly. $\gamma = 0$ in eq. (37) yields

$$\frac{\partial A}{\partial \tau_1} = \pm\sqrt{8}\,(A^2 + C)\,. \tag{40}$$

Defining

$$W = +\sqrt{|C|}\,,$$

$$\sigma = \frac{\dot{A}_0}{|\dot{A}_0|} = sign(\dot{A}_0)\,,$$

$$\tau = \sigma\sqrt{8}\,W\,\tau_1 = \sigma\sqrt{8}\,W\,\epsilon\,t\,, \tag{41}$$

we write the solution of eq. (40) corresponding to the initial conditions

$$A = A_0 \qquad \dot{A} = \dot{A}_0 \qquad at \quad \tau_1 = \tau = t = 0$$

in the form

$$\tau = arctg\frac{A}{W} - arctg\frac{A_0}{W} \qquad for \quad C\ positive\,, \tag{42}$$

$$\tau = \frac{1}{2}\,ln\Big(\frac{A-W}{A+W}\cdot\frac{A_0+W}{A_0-W}\Big) \qquad for \quad C\ negative\,. \tag{43}$$

This allows us to determine the explosion time $t_e$ by inserting $A = \pm\infty$ :

$$t_e = \frac{1}{\sqrt{8}\,W\,|\epsilon|}\Big(\frac{\pi}{2} - s\,arctg\frac{A_0}{W}\Big) \qquad for \quad C\ positive\,, \tag{44}$$

$$t_e = -\frac{s}{2\sqrt{8}\,W\,|\epsilon|}\,ln\Big(\frac{A_0-W}{A_0+W}\Big) \qquad for \quad C\ negative\,, \tag{45}$$

with

$$s = sign(\epsilon\,\dot{A}_0)\,.$$

The $t_e$ values resulting from eq. (45) are real due to $C > -A_0^2$ , which follows from eqs. (35-36).
For positive $C$ there are always poles at positive times $t$.
For negative $C$ only one pole exists. For negative $t_e$ the solution does not explode at positive times.
For $C \to 0$ one gets the Cherry-like solutions (21) and (39).

## 2.3 Remarks on solutions with $\gamma \neq 0$

In general, $\gamma$ and $C$ are non-zero. The exact solution of eq. (37) can be presented by means of elliptic functions; however, the discussion of stability can be done much more simply by using the potential given by eq. (38). We interpret eq. (37) as the energy of a "particle" in the potential $V$ of eq. (38); $A$ is its co-ordinate and $\dot{A}$ its velocity. The energy vanishes, hence the "particle" must not enter any region with positive $V$. The essential difference to usual potential problems in classical mechanics is that the potential (38) depends via $C$ on the initial velocity $\dot{A}_0$.

The potential (38) has three zeros with respect to $A^2$ of which at least one is real and positive. For

$$A^2 > A^2_{min} \tag{46}$$

the potential is negative, which means an allowed region. For $C > 0$ this is the only real zero of $V$. For $C < 0$ there are two additional real zeros. But for these $A^2 + C < 0$ must hold, which is forbidden because of eq. (35).

Figure 2 presents six examples of the potential $V$ versus $A$. We discuss here only the cases with $\gamma \neq 0$. The behaviour of the moving "particle" essentially depends on the direction of its initial velocity $\dot{A}_0$:

- If $\epsilon \dot{A}_0 > 0$ , the "particle" runs downwards and explosion occurs.
- If $\epsilon \dot{A}_0 < 0$ , the "particle" climbs upwards for some time, in Fig. 2 in left direction, until it is reflected at $A = A_{min}$, where the gradient $dV/dA$ is negative. Therefore the particle returns, runs downwards and explosion occurs.

Thus we expect explosion of all solutions with $\gamma \neq 0$.

# 3 Comparison between first-order multiple time scale solutions and numerical solutions

The first-order multiple time scale solutions - labeled "first-order solutions" for short - are given by eqs. (8), (10) and (19). In this section we compare for some examples the first-order solutions with the corresponding numerical solutions of differential equation (7). We keep the notation $x$, $y$ for the numerical solutions and write $u$, $v$ instead of $x$, $y$ for the first-order solutions:

$$u + i\,v \;=\; \zeta_0 \;+\; \epsilon\,\zeta_1 \;,$$

where $\zeta_0$ determines via $a_+$, $a_-$ the explosion time or, if there is no explosion, the stability; $\zeta_1$ influences the phase.

Let us look for an adequate representation of the results.
Figure 4 shows the numerically obtained solution $x(t)$ , $y(t)$ (solid) and the first-order solution $u(t)$ , $v(t)$ (dotted) versus time for one example. $x$, $y$, $u$ and $v$ contain oscillations with both frequencies $\omega_-$ and $\omega_+$; superpositioning them leads to rather noisy curves.
Figure 5 shows the same example as Fig. 4. The simpler curves in Fig. 5 are obtained by plotting the absolute values

$$r = \sqrt{x^2 + y^2} \qquad , \qquad \rho = \sqrt{u^2 + v^2} \;, \tag{47}$$

which oscillate essentially only with the frequency

$$\omega_+ \;-\; \omega_- \;=\; \omega_- \;.$$

Most of the figures therefore show $r(t)$ and $\rho(t)$ .

## 3.1 Input of the initial conditions

The initial conditions for $x = u$, $y = v$, $\dot{x} = \dot{u}$, $\dot{y} = \dot{v}$ at $t = 0$ can be expressed in terms of initial values of $a_+$ and $a_-$ :

$$\zeta \;=\; \Big(a_+ \;+\; a_-\Big)_{\tau_1=0} \tag{48}$$

and

$$\dot{\zeta} = -i\left(\omega_+ a_+ + \omega_- a_-\right)_{\tau_1=0} + \epsilon\left(\frac{\partial a_+}{\partial \tau_1} + \frac{\partial a_-}{\partial \tau_1}\right)_{\tau_1=0},$$

which upon use of eq. (20) becomes

$$\dot{\zeta} = -i\left(\omega_+ a_+ + \omega_- a_-\right)_{\tau_1=0} + i\sqrt{2}\,\epsilon\left(a_-^2 - 2\,a_+ a_-^*\right)_{\tau_1=0}. \qquad (49)$$

Starting time is $t = 0$ ; with $A_0 = A$ at $t = 0$ etc.
The examples are defined by the parameters $\epsilon$ , $A_0$ , $\dot{A}_0$ , $\phi_0$ and $\gamma$, from which $a_+$ and $a_-$ are obtained via eq. (25) and the first of the eqs. (20).

## 3.2 Cherry-like cases

The Cherry-like cases are defined by $\epsilon$ , $T$ and $\varphi$ ; see eq. (39).

Let us consider Figs. 5-7. The solid curve is the numerically obtained $r$ versus time and one of the dotted curves is the absolute value

$$\rho = |\zeta_0 + \epsilon\,\zeta_1|$$

of the first-order solution. Its behaviour is similar to that of the zero-order solution

$$|\zeta_0| = \frac{1}{2\,(T - \epsilon\,t)}\sqrt{\frac{3}{2} + \sqrt{2}\,sin(\varphi - \frac{t}{\sqrt{2}})}, \qquad (50)$$

which follows by inserting the Cherry solution (21) for $a_+$ , $a_-$ and the frequency (16) into eq. (10) for $\zeta_0$. From eq. (50) we expect broad maxima and narrow minima because the square root is steeper for small values of the argument than for large ones. Replacing the *sin* by $\pm 1$ yields

$$\rho_{max} = \frac{0.85}{T - \epsilon\,t} \qquad (51)$$

approximating the envelope for the relative maxima (dotted) and

$$\rho_{min} = \frac{0.15}{T - \epsilon\,t}, \qquad (52)$$

for the relative minima. The zero-order solution (50) differs from the first-order solution by about 5-30%.
The explosion time is

$$t_e = \frac{T}{\epsilon}. \qquad (53)$$

Figures 5-7 start with the initial value $T = 1$; hence the explosion time is $1/\epsilon$;
this roughly describes the explosion time in all examples with initially $x^2+y^2$ and $\dot{x}^2 + \dot{y}^2$ of order 1. This is the case in our examples; hence the time $1/\epsilon$ is noted in our plots.

The numerical solution agrees more or less well with the first-order solution until the latter explodes. Near the explosion time the numerical solution reaches the saddle curve

$$\frac{1}{2}\,(x^2 + y^2) + \frac{4\epsilon}{3}\,x^3 = \frac{1}{96\,\epsilon^2} \tag{54}$$

also called "separatrix" because it separates the
"outer" region with open $U = const$ lines from the
"inner" region with closed $U = const$ lines around the top of the hill at $x = y = 0$; see Fig. 1; $U$ is the potential given by eq. (5).
The separatrix cuts the $x$-axis at the saddle point

$$x = -\frac{1}{4\,\epsilon} \tag{55}$$

and at

$$x = \frac{1}{8\,\epsilon}\,. \tag{56}$$

After general features let us now discuss some examples:
Figure 5 has input data causing the particle on the hill to enter the separatrix near the saddle point, where the electric "hill force" is much weaker than the magnetic one, and hence for $t > 1/\epsilon$ the motion is a gyration with drift. From eq. (15)-(16) the gyration frequency is about

$$B \approx 3\,\omega_-\,,$$

where $\omega_-$ is the frequency of the $r$ oscillation for small $t$ values, as can be seen from the distance of adjoining relative $r$ maxima in Fig. 5. After the drift has carried the particle far enough away from the saddle point, the particle runs away exponentially, as described in Appendix A.

Figure 6 shows that the particle on the hill for appropriately chosen values of the parameters can be"reflected" near the separatrix (54). After the

explosion of the first-order solution at $1/\epsilon$ the oscillation amplitude of the numerical solution decreases until, say, $t \approx 2/\epsilon$. Then the oscillation amplitude increases again; this we call "second start".

Figure 7 shows $r(t)$ and $\rho(t)$ for an $\epsilon$ value smaller than in Figs. 5 and 6; hence the time interval of agreement of the numerical and first-order solutions covers much more oscillations than in the case of Fig. 5 and 6. As in Fig. 5, the particle reaches the separatrix (54) near the saddle point. The gyration oscillations, however, exceed the frame of Fig. 7 and therefore cannot be seen; we present them in the following figure.

Figure 8 shows the orbit of the particle in the $x$-$y$ plane; the input data are the same as for Fig. 7. The particle starts near the centre, spirals outward and reaches the separatrix (dotted) near the saddle point. In this region the motion is a gyration with drift causing some loops, until the drift carries the particle far enough away from the saddle point; after this it runs away exponentially as described in Appendix A.

Figure 9 shows an example with negative $\epsilon$ and negative explosion time. The numerical and first-order solutions agree for times $< 1/|\epsilon|$. After this time the first-order solution decreases according to eq. (50) for the zero-order solution $\zeta_0$; the first-order term $\zeta_1$ essentially influences only the phase. Although the first-order solution is stable for all positive times, the numerical solution increases und runs away. This different behaviour becomes plausible when the energy of the numerical and first-order solution are compared. The energy of the particle on the hill

$$E = \frac{1}{2}\left(\frac{dx}{dt}\right)^2 + \frac{1}{2}\left(\frac{dy}{dt}\right)^2 - \frac{1}{2}x_2 - \frac{1}{2}y^2 - \frac{4\epsilon}{3}x^3$$

is a constant of motion and positive in the case of Fig. 9. The positive energy together with the non-linear term in eq. (7) causes the particle on the hill after sufficiently large times to spiral outwards in the $x$-$y$ plane and run away exponentially, similarly to the case in Fig. 8.
Let us estimate the energy in first-order approximation by replacing $d/dt$ by $\omega_-$ or $\omega_+$ and $x, y$ by $a_+$ or $a_-$. Inserting the Cherry solution (21) yields

$$E_{app} \sim \frac{1}{(T - \epsilon\, t)^2} = \frac{1}{(T + |\epsilon\,|t)^2}\,,$$

which goes to zero with increasing time in contradiction to the energy conservation mentioned above. This means that the particle described by the first-order solution asymptotically approaches the top $x = y = 0$ of the hill similarly to some zero-energy solutions.

### 3.3 Non-Cherry-like solutions

The case of positive parameters $A_0$, $\dot{A}_0$ and $\epsilon$ roughly corresponds to the Cherry-like Figs. 4-8 and is not discussed here. Therefore we restrict ourselves to some cases with negative $\epsilon$.

Figure 10 is an example of $\gamma = 0$ and positive $C$ with a first-order solution (42) exploding at the time given by eq. (44). For $A_0 < \dot{A}_0$ the numerical solution runs away after the explosion of the first-order-solution, qualitatively similarly to the "second start" in Fig. 5.

Figure 11 is an example of $\gamma = 0$ and negative $C$ and $\epsilon$. The first-order solution (43) explodes at the negative time given by eq. (45) and goes $\rightarrow W$ for increasing positive time. From this one might incorrectly conclude that also the numerical solution should be stable for all positive times. This is, however, not the case:
Numerical and first-order solutions agree for, say, $t < 1/|\epsilon|$; after this the numerical solution increases and runs away. The reason for this discrepancy is the artificial symmetry introduced by the time averaging procedure in Sec. 2, causing the first-order solution to circulate around the top of the hill at a distance of order $W$. In reality, however, there is no symmetry; hence the numerical solution may spiral outwards in the $x$-$y$ plane und run away for sufficiently large times, as in the examples of Figs. 9 and 11.

Figure 12 differs from Fig. 11 by a small $\gamma$-value $\neq$ zero, which causes the first-order solution to explode near

$$t_e \approx -\frac{ln|\gamma|}{|\epsilon|\sqrt{-2C}} \tag{57}$$

(see Appendix B, eq. (B8)).

In all cases we have numerical solutions which run away exponentially for large enough times. If the initial values are of order 1, the numerical and

first-order solutions agree more or less well up to times about $1/|\epsilon|$ (marked in the figures). The amplitudes decrease due to the negative $\epsilon$ and increase again after becoming minimal. For negative $\epsilon$ and positive initial values $A_0$ and $\dot{A}_0$ (as in Figs. 9-11) there is no connection between the explosion of the first-order solution and the transition of the numerical solution from closed to open $U = const$ lines (as in Fig. 5).

# References


[1] T. M. Cherry, Trans. Cambridge Philos. Soc. **23**, 199, (1925);
see E.T. Whittaker, Analytical Dynamics (Cambridge, London, 1937), Sec. 182, p. 142;
and A. Wintner, The Analytical Foundations of Celestial Mechanics, (Princeton University, Princeton, 1947), Sec. 136, p. 101

[2] D. Pfirsch, Z. Naturforsch. **45a**, 839 (1990)

[3] Jahnke-Emde, Tables of Higher Functions, Teubner 1948

# Figures

Fig. 1
Solid: Equidistant contour lines of the potential

$$U(x,y) \;=\; -\,\frac{1}{2}\,(x^2 \,+\, y^2) \;-\; \frac{4\epsilon}{3}\,x^3 \qquad (s.5)$$

in the $x$-$y$ plane. The small quasi-circle near the top of the hill at $x = y = 0$ has the same height ($U$-value) as the line at the left edge of the figure. Further left the absolute value of the potential grows rapidly.

Dotted: the saddle curve of eq. (54)
with saddle point S left at $x = -1/4\epsilon$ .

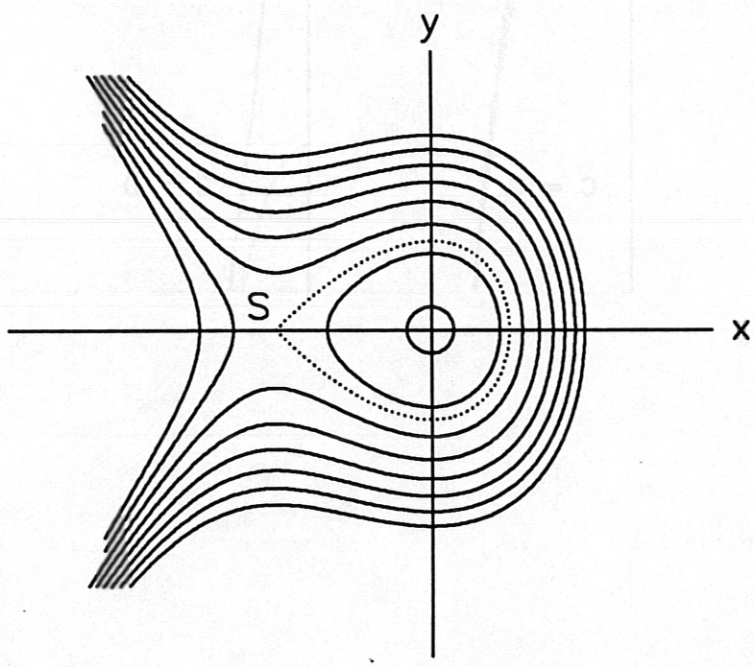

Fig. 2

The potential V(A) from eq. (38) vs. $A$
for $\gamma \neq 0$ (solid) and $\gamma = 0$ (dashed) .
For details concerning $\gamma \neq 0$ and $C < 0$ see Fig. 3.

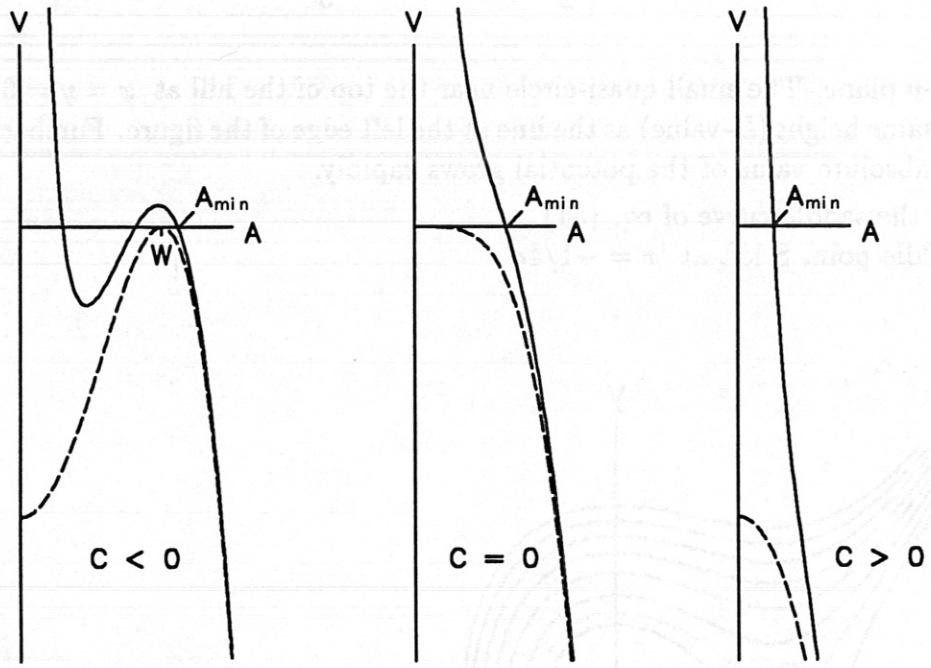

Fig. 3
Square roots of the contributions to the potential $V$ (s. eq. (38)) vs. $A$ and the zeros of $V(A)$ for

$\gamma/\sqrt{2} = 0.6\,, \qquad C = -1\,, \qquad W = \sqrt{|C|} = 1\,.$

Solid: $2\,|A^2 - W^2|$ vs. $A$.
Dotted: $\gamma/\sqrt{2}\,A$ vs. $A$.

The cutting points are the zeros of $V(A)$.
The particle starts at $A > A_{min}$ and goes left until $A_{min}$, which is the largest zero. Then it runs right and explosion occurs.

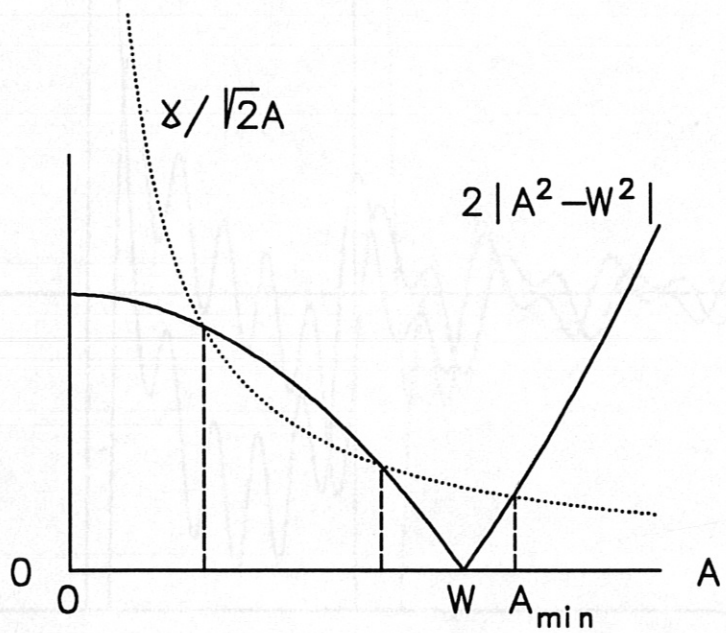

Fig. 4

$x$ , $y$ (numerical, solid) and

$u$ , $v$ (first-order solution, dotted)

vs. time for the Cherry-like case:

$\epsilon = 0.03$ ,

$\varphi = 0.8$ ,

$T = 1.0$ .

The dotted vertical lies at $t = t_e = 1/\epsilon$ .

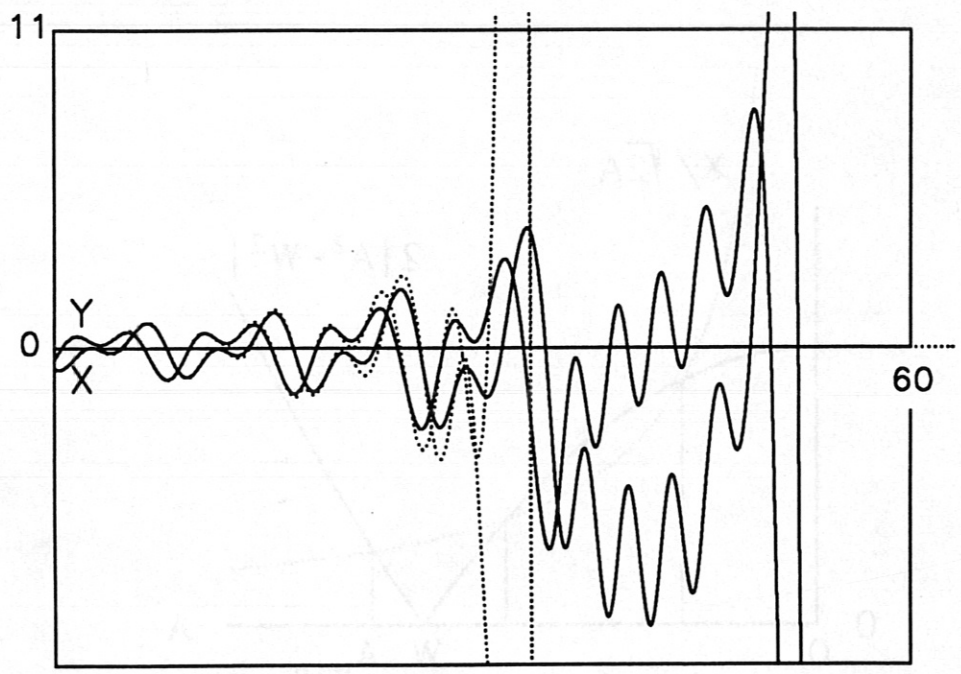

Fig. 5

$r = \sqrt{x^2 + y^2}$ (numerical, solid) ,

$\rho = \sqrt{u^2 + v^2}$ ( first-order solution, dotted) and

the envelope $\rho_{max}$ (dotted, eq. (51)) vs. time for the Cherry-like case

$\epsilon = 0.03$ ,

$\varphi = 0.8$ ,

$T = 1.0$ .

The data are the same as in Fig. 4.

The first-order solution explodes at $t = 1/\epsilon$.

The oscillations at $t > 1/\epsilon$ stem from the gyration near the saddle point.

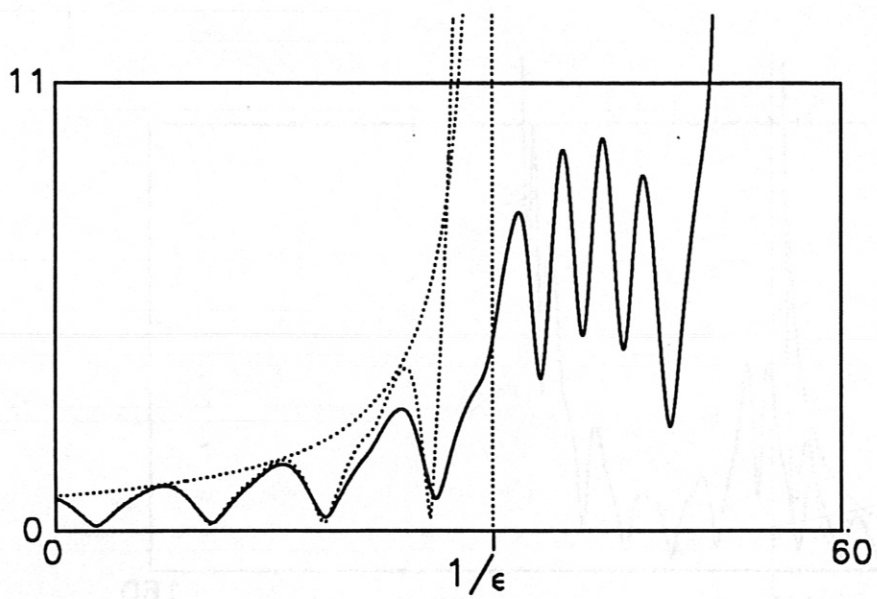

Fig. 6
$r$ (numerical, solid) , $\rho$ ( first-order solution, dotted) and
the envelope $\rho_{max}$ (dotted, eq. (51)) vs. time for the Cherry-like case
$\epsilon = 0.03$ ,
$\varphi = 0.$ ,
$T = 1.0$ .

The data are the same as in Fig. 5, except for $\varphi$ .
This example shows that the particle on the hill for appropriately chosen values of the parameters can be "reflected" near the saddle point. Its oscillation amplitude decreases until, say, $t \approx 2/\epsilon$ and increases again after this.

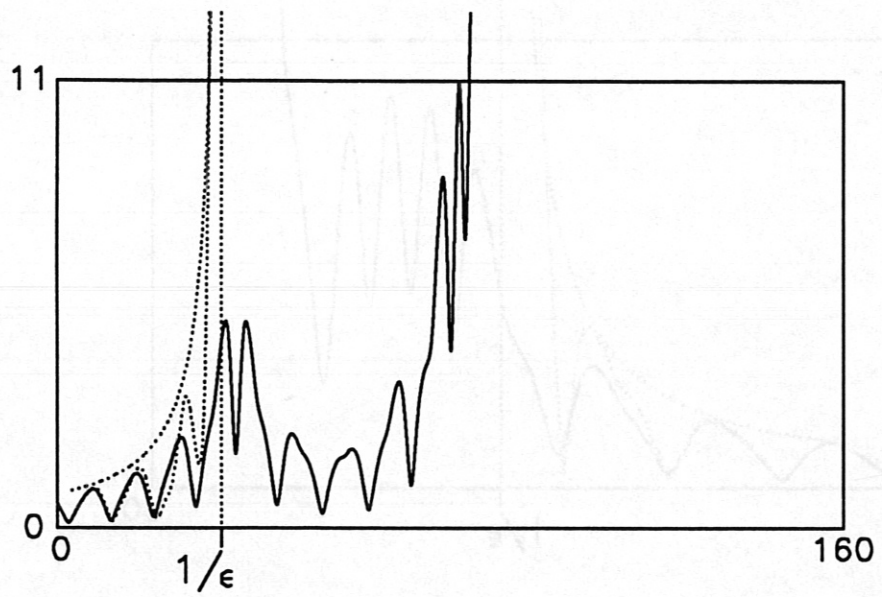

Fig. 7
$r$ (numerical, solid) , $\rho$ ( first-order solution, dotted) and
the envelope $\rho_{max}$ of eq. (51) vs. time for the
Cherry-like case
$\epsilon = 0.01$ ,
$\varphi = 0.$ ,
$T = 1.0$ .

The data are the same as in Fig. 6, except for $\epsilon$.
No reflection or second start is found.

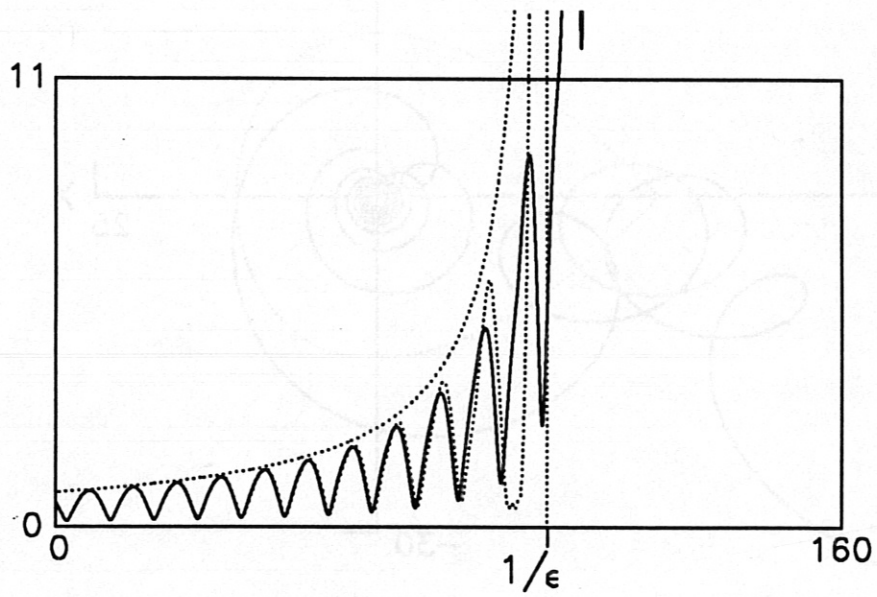

Fig. 8
Orbit (numerical) of the particle on the hill in the $x$-$y$ plane
for the Cherry-like case of Fig. 7 (solid).
The dotted line is the saddle curve of eq. (54).

The particle starts near the centre and surrounds the centre until it comes near the saddle point, where the electric force is much weaker than the magneitic one and the motion is a gyration with drift. Bottom-left the solution becomes exponential according to eq. (A2b) in Appendix A.

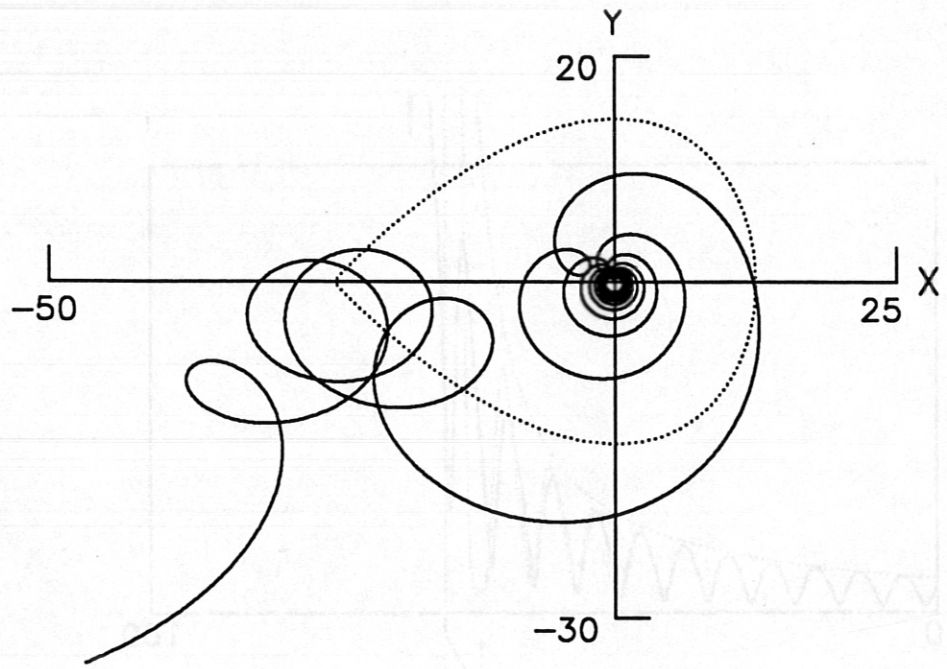

Fig. 9
$r$ (numerical, solid) , $\rho$ (first-order solution, dotted)
and its envelope eq. (51) (dotted) vs. time for the Cherry-like case
$\epsilon = -0.01$ ,
$\varphi = 2.3562$ ,
$T = 0.354$ .

The explosion time $t_e = -35.4$ is negative, hence the first-order solution does not explode at positive times but goes to zero with increasing time according to eq. (51).

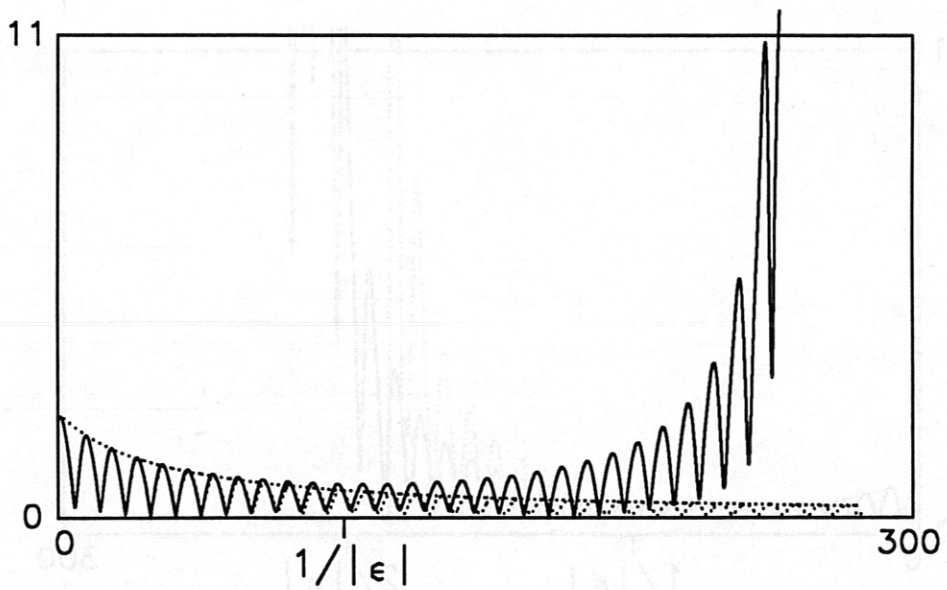

Fig. 10
$r$ (numerical, solid) and $\rho$ ( first-order solution, dotted) vs. time for
$\epsilon = -0.01$ ,
$A_0 = 0.4$ ,
$\dot{A}_0 = 1.0$ ,
$\phi_0 = 0.0$ ,
$\gamma = 0.0$ .

For $A_0 < \dot{A}_0$ the numerical solution runs away after the explosion of the first-order solution, qualitatively similarly to the Cherry-like cases of the foregoing figures.

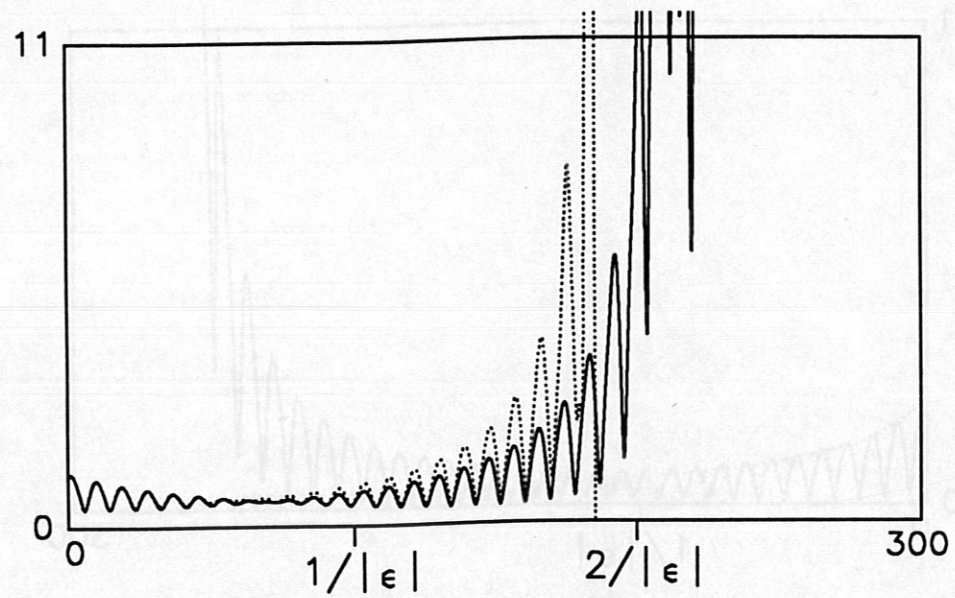

Fig. 11
$r$ (numerical, solid) and $\rho$ ( first-order solution, dotted) vs. time for
$\epsilon = -0.01$ ,
$A_0 = 1.0$ ,
$\dot{A}_0 = 0.4$ ,
$\phi_0 = 0.0$ ,
$\gamma = 0.0$ .

In the case of $A_0 > \dot{A}_0$ and $\gamma = 0$ the first-order solution does not explode due to violation of energy conservation in first-order approximation.

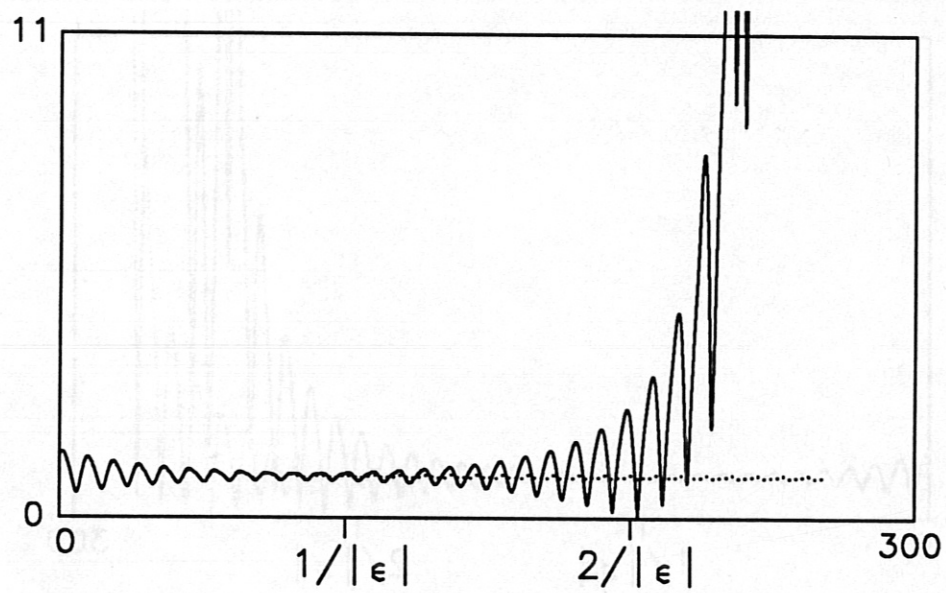

Fig. 12
$r$ (numerical, solid) and $\rho$ ( first-order solution, dotted) vs. time for
$\epsilon = -0.01$ ,
$A_0 = 1.0$ ,
$\dot{A}_0 = 0.4$ ,
$\phi_0 = 0.0$ ,
$\gamma = 0.002$ .

The data are the same as for Fig. 11 - except for the the small $\gamma$ value causing the first-order solution to explode near $t = 2.8/|\epsilon|$.

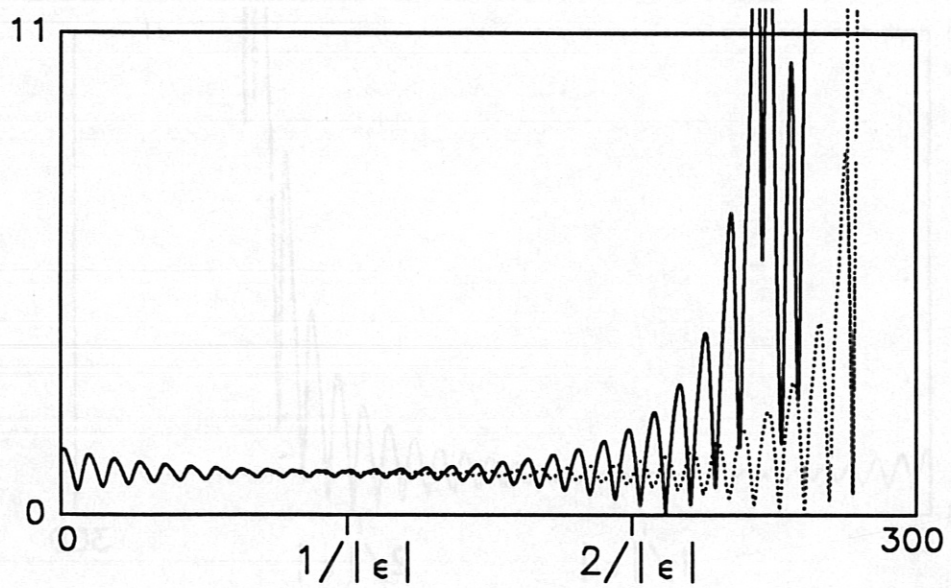

# Appendix A

## Asymptotic Behaviour

We investigate the behaviour of the solutions of the equations of motion

$$\ddot{x} - B\,\dot{y} - x = 4\,\epsilon\,x^2\,,$$

$$\ddot{y} + B\,\dot{x} - y = 0 \qquad (A1)$$

for very large values of $|x|$ , $|y|$ , $|\dot{x}|$ and $|\dot{y}|$.
Two classes of asymptotic behaviour are as yet found numerically:

a) Exploding solutions

$$y = -\frac{3B/2}{\epsilon\,(t-t_0)}\,,$$

$$x = \frac{3/2}{\epsilon\,(t-t_0)^2}\,. \qquad (A2a)$$

b) Exponentially increasing solutions

$$y = -\frac{4}{B}\,\epsilon\,e^{t-t_0}\,,$$

$$x = -\,e^{(t-t_0)/2}\,. \qquad (A2b)$$

$t_0$ is a constant of integration.

Relevance to multiple time scale formalism

The initial conditions relevant to comparison with multiple time scale approximations can be characterized by

$$x_0^2 + y_0^2 \quad and \quad \dot{x}_0^2 + \dot{y}_0^2 << \frac{1}{|\epsilon|}\,; \qquad (A3)$$

we therefore ask for the initial conditions leading to the explosive case and test whether - or not - these coincide with eq. (A3). The general answer is very complicated; we therefore restrict ourselves to a special class of initial conditions.

Special initial condition

In the explosive case the particle must reach large positive $x$ values; therefore we regard a 1-D class of initial conditions with variable $x_0$ and fixed initial velocity $\dot{x}_0; \dot{y}_0$ and initial $y_0$. We choose

$$x = x_0 \quad , \quad y = \dot{x} = \dot{y} = 0 \quad at \quad t = 0 \, . \tag{A4}$$

Furthermore, we get rid of the parameter $\epsilon$ by inserting

$$\xi = 4\epsilon \, x \, , \qquad \eta = 4\epsilon \, y$$

into eq. (A1). This yields

$$\ddot{\xi} \, - \, B \, \dot{\eta} \, - \, \xi \, = \, \xi^2 \, ,$$

$$\ddot{\eta} \, + \, B \, \dot{\xi} \, - \, \eta \, = \, 0 \, ,$$

which is equivalent to eq. (A1) for $\epsilon = 1/4$. (A5)

Figure 13 shows numerical solutions to system (A1+A4+A5) for some initial values near $x_0 = 1$. It seems that there is a singular solution separating solutions running away into the negative $x$-direction, such as (A2b) from exploding solutions running away into the positive $x$-direction. The explosion time of the solution to system (A1+A4+A5) is within the plot inaccuracy of Fig. 14:

$$t_0 \, \approx \, 2.98 \, \frac{(1 - 1.0205/x_0)^{-0.06}}{\sqrt{x_0}} \, , \tag{A6}$$

and hence there is no explosion for $x_0 < 1.0205$ . (A7)

The separatrix (54) cuts the positive $x$-axis at $x = 0.5$; hence the interval with exploding solutions is of no relevance to multiple time scale approximations.

Fig. 13
$x$ vs. time for the initial condidtion used in Appendix A

$x = x_0 \quad , \quad y = \dot{x} = \dot{y} = 0 \quad at \quad t = 0$

for 4 different $x_0$ values.

It seems that there is a singular solution separating explosive solutions exceeding the upper plot frame from exponentially increasing ones going to negative $x$ values with increasing time.

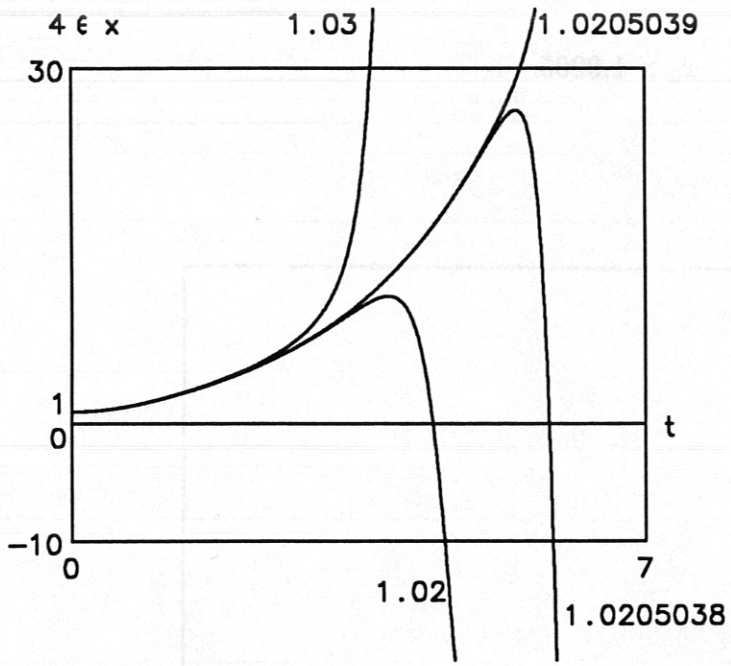

Fig. 14
Explosion time $t_0$ vs. $x_0$, square root scaled,
for the initial condition used in Appendix A

$x = x_0 \quad , \quad y = \dot{x} = \dot{y} = 0 \quad at \quad t = 0.$

Solid: the interpolation formula

$$t_0 \approx 2.98 \frac{(1 - 1.0205/x_0)^{-0.06}}{\sqrt{x_0}} , \qquad (s.A6)$$

Rhombuses: values obtained by solving the differential equation (A1) numerically.

Explosion occurs for $x_0 > 1.0205$.

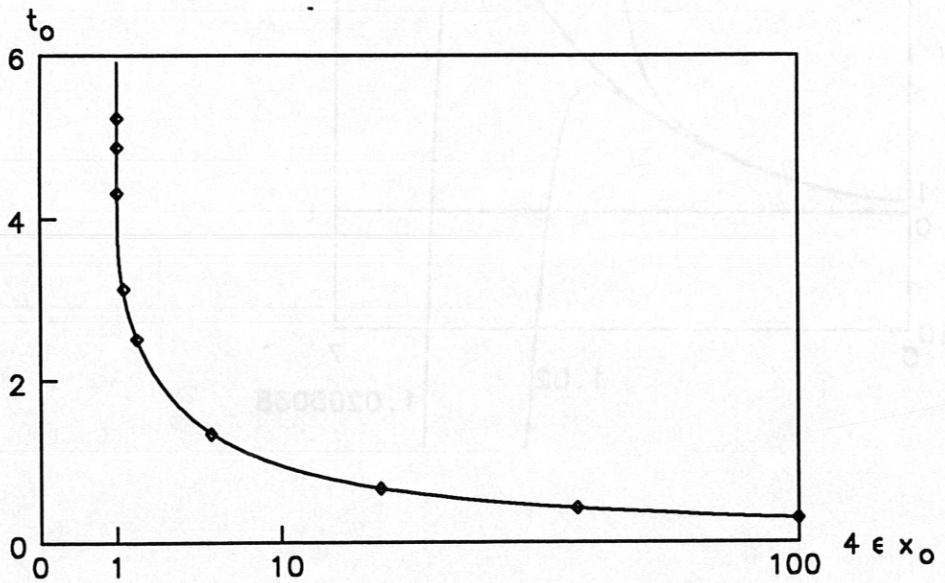

Large initial values $x_0$

For very large $x_0$ values one can derive rule (A6) also analytically. In this case eq. (A1) reduces to

$$\ddot{x} \;=\; x^2 \;,$$

which yields together with initial condition (A4)

$$\frac{1}{2}\dot{x}^2 \;=\; \frac{1}{3}(x^3 - x_0^3) \;.$$

Introducing

$$\tau = t\,\sqrt{\frac{2}{3}\,x_0} \qquad and \qquad X \;=\; \frac{x}{x_0} \tag{A8}$$

yields

$$\frac{dX}{d\tau} \;=\; \sqrt{X^3 - 1} \qquad , \qquad X(\tau = 0) \;=\; 1 \;,$$

which gives

$$\tau \;=\; \int_1^X \frac{dU}{\sqrt{U^3 - 1}} \;=\; 2.43 \quad for\; X \to \infty \;; \tag{A9}$$

the case $X \to \infty$ corresponds to the explosion time.
From eq. (A8+A9) one gets the explosion time

$$t_0 \;=\; 2.43\,\sqrt{\frac{3}{2\,x_0}} \;=\; \frac{2.98}{\sqrt{x_0}} \tag{A10}$$

in agreement with rule (A6) for large $x_0$.
The evaluation of integral (A9) may be done numerically or by means of the relation

$$\int_1^\infty \frac{dU}{\sqrt{U^3 - 1}} \;=\; 2 \;\times\; 3^{-1/4} \;\times\; F(\alpha = 15^0 \;,\; \varphi = 90^0) \;,$$

where $F = 1.5981$ is the elliptic integral of the first kind; see, for example, [3] .

## Appendix B

## Explosion for $\gamma \neq 0$

Let us estimate the explosion time for the class of solutions with

$$C = -W^2 \quad , \quad A \; positive \quad , \quad \gamma << 1 \quad , \quad sign(\epsilon \dot{A}_0) \; negative \quad (B1)$$

corresponding to the non-exploding solutions (43) with $\gamma = 0$. For non-vanishing $\gamma$ the potential $V$ has a relative maximum near $A = W$ and a hollow for $A < W$. From eq. (46) the "particle" cannot enter the potential hollow at $A < W$ and must move along the slope $A \geq W$. In case (B1) the "particle" quickly runs upwards until the region

$$A \approx W$$

is reached, where it moves more slowly. Then $A - W$ and $\gamma$ are both small quantities; expanding eq. (37) up to lowest order yields the differential equation

$$\frac{dA}{dt} = -E\sqrt{(A-W)^2 - G^2} \qquad (B2)$$

with

$$G = \frac{\gamma}{\sqrt{32}\, W^2} \qquad (B3)$$

and

$$E = \sqrt{32}\, |\epsilon|\, W \, , \qquad (B4)$$

which approximatively describes the motion of the particle in the region $A \approx W$. We write the solution of eq. (B2) in the form

$$A = W + \frac{1}{2} G^2 \, e^{E(t-t_0)} + \frac{1}{2} \, e^{-E(t-t_0)} \, , \qquad (B5)$$

with

$$t_0 \approx \frac{ln(2(A_0 - W))}{E} \qquad (B6)$$

following from the initial condition and the assumption of small $\gamma$. The term with $G^2$ runs away exponentially until the range of validity of approximation (B2-B5) is exceeded. For sufficiently large $A$ values eq. (37) approximatively becomes

$$\frac{dA}{dt} \approx \sqrt{8}\, \epsilon \, A^2 \, ,$$

which has a solution exploding shortly after exceeding the range of validity of approximation (B2-B5). Defining this range rather arbitrarily by

$$A(t_e) = 2\,W \tag{B7}$$

and inserting eqs. (B5) and (B6) into eq. (B7) gives

$$t_e \;=\; \frac{1}{E}\left(\,4.8 \;+\; ln\,(A_0 - W) \;+\; 5\;ln\,W \;-\; 2\;ln|\gamma|\right), \tag{B8}$$

which roughly approximates the explosion times obtained by solving eq. (37) numerically.